

## EQUATION OF STATE AND OPACITIES FOR HYDROGEN ATMOSPHERES OF MAGNETARS

ALEXANDER Y. POTEKHIN<sup>1</sup>

Ioffe Physico-Technical Institute, Politekhnikeskaya 26, 194021 St. Petersburg, Russia; palex@astro.ioffe.ru

AND

GILLES CHABRIER

École Normale Supérieure de Lyon, Centre de Recherche Astrophysique de Lyon, UMR CNRS  
No. 5574, 46 allée d'Italie, 69364 Lyon Cedex 07, France; chabrier@ens-lyon.fr

Received 2003 June 26; accepted 2003 September 9

### ABSTRACT

The equation of state and radiative opacities of partially ionized, strongly magnetized hydrogen plasmas, presented in a previous paper for the magnetic field strengths,  $8 \times 10^{11} \text{ G} \lesssim B \lesssim 3 \times 10^{13} \text{ G}$ , are extended to the field strengths,  $3 \times 10^{13} \text{ G} \lesssim B \leq 10^{15} \text{ G}$ , relevant for magnetars. The first- and second-order thermodynamic functions and radiative opacities are calculated and tabulated for  $5 \times 10^5 \text{ K} \leq T \leq 4 \times 10^7 \text{ K}$  in a wide range of densities. We show that bound-free transitions give an important contribution to the opacities in the considered range of  $B$  in the outer neutron star atmosphere layers. Unlike the case of weaker fields, bound-bound transitions are unimportant.

*Subject headings:* equation of state — magnetic fields — plasmas — stars: atmospheres — stars: neutron

*On-line material:* color figures

### 1. INTRODUCTION

Neutron star atmospheres differ from the atmospheres of ordinary stars because of the high gravity and magnetic fields present there. The majority of the known pulsars possess magnetic fields  $B \sim 10^{11} - 10^{13.5} \text{ G}$  (R. Manchester et al. 2003, in preparation)<sup>2</sup>. Most popular models of the soft gamma repeaters and anomalous X-ray pulsars assume they are *magnetars*, neutron stars with superstrong magnetic fields,  $B \sim 10^{14} - 10^{15} \text{ G}$  (e.g., Thompson 2003).

The properties of matter are strongly modified if the electron cyclotron energy  $\hbar\omega_{ce} = \hbar eB/m_e c$  exceeds 1 a.u.—i.e., the field strength  $B$  is higher than  $B_0 = m_e^2 c^3 / \hbar^3 = 2.3505 \times 10^9 \text{ G}$  (for a review, see Lai 2001). Shibano et al. (1992) presented the first detailed model of hydrogen atmospheres for neutron stars with strong magnetic fields. Later it was developed and used by many authors (e.g., Zavlin et al. 1995; Pavlov et al. 1995; Page, Shibano, & Zavlin 1996; Zane et al. 2001; Ho & Lai 2003; Özel 2003; and references therein). These works have played a valuable role in assessing the observed spectra of neutron stars. Despite the recognition of the possibility that the absorption by atoms can significantly contribute to the opacities, the atoms were not included in the atmosphere model in a thermodynamically consistent manner in the listed works.

The theoretical equation of state for partially ionized hydrogen plasma with strong magnetic fields was developed by Potekhin, Chabrier, & Shibano (1999). The nonperturbative effects of atomic thermal motion across the magnetic field were taken into account and shown to be important. Based on this theory, in a previous paper (Potekhin & Chabrier 2003, hereafter Paper I), we performed extensive calculations of the thermodynamic functions and calculated monochromatic and Rosseland mean opacities, taking into account the bound-

bound and bound-free transitions. These calculations were done at  $11.9 \leq \log B[\text{G}] \leq 13.5$ . In addition, we reevaluated the free-free opacities, taking into account the motion of both interacting particles, electron and proton, in arbitrary magnetic fields.

Here we report an extension of the previous calculations of the equation of state and opacities of a partially ionized hydrogen plasma to higher field strengths,  $13.5 \leq \log B[\text{G}] \leq 15$ .

### 2. THEORETICAL MODEL

A major complication when incorporating bound species in the models of strongly magnetized neutron star atmospheres arises from the strong coupling between the center-of-mass motion of the atom and the internal atomic structure. If an atom rests without motion in a strong magnetic field, there are two distinct classes of its quantum states: at every value of the Landau quantum number  $n$  and the magnetic quantum number  $-s$  ( $n \geq 0$ ,  $s \geq -n$ ), there is one tightly bound state with binding energy growing asymptotically (at  $B \rightarrow \infty$ ) as  $(\ln B)^2$ , and an infinite series of loosely bound states (numbered by  $\nu = 0, 1, \dots$ ) with binding energies approaching the energies of a field-free H atom (e.g., Canuto & Ventura 1977). The Landau number  $n$  is not a good quantum number, in the sense that the Coulomb interaction mixes different Landau orbitals of a free electron, but this numbering is unambiguous and convenient at  $B \gg B_0$ . The atom is elongated: its size along the magnetic field  $\mathbf{B}$  either decreases logarithmically (for the tightly bound states) or remains nearly constant (for the loosely bound states), while the transverse radius decreases as  $B^{-1/2}$ . The radiative transition rates are different for the three basic polarizations: the linear polarization along the field and the two circular polarizations in the transverse plane.

This simplicity is destroyed when atomic motion is taken into account. The electric field induced in the comoving frame of reference breaks down the cylindrical symmetry. Separating the center-of-mass motion and choosing an appropriate gauge of

<sup>1</sup> Also at the Isaac Newton Institute of Chile, St. Petersburg Branch, Russia.

<sup>2</sup> See the ATNF Pulsar Catalogue at <http://www.atnf.csiro.au/research/pulsar/psrcat>.

the vector potential (Gor'kov & Dzyaloshinskii 1967; Vincke, Le Dourneuf, & Baye 1992; Potekhin 1994), one comes to an effective one-particle Schrödinger equation with an effective Hamiltonian depending on the pseudomomentum  $\mathbf{K}$ , which is a conserved quantity related to the center-of-mass motion in a magnetic field. If the component of  $\mathbf{K}$  perpendicular to  $\mathbf{B}$ ,  $K_{\perp}$ , is finite, then not only  $n$ , but also  $s$  is not a good quantum number; nevertheless, it is convenient to retain the quantum level numbering,  $n$ ,  $s$ , and  $\nu$ , specified above. In the adiabatic approximation widely used in the past (Gor'kov & Dzyaloshinskii 1967; Ipatova, Maslov, & Subashiev 1984), the transverse part of the wave function is postulated to be the same as for an electron without Coulomb interaction. We perform calculations without this approximation, using the techniques described by Potekhin (1994) for the discrete atomic spectrum and by Potekhin & Pavlov (1997) for the continuum. This technique uses the basis of Landau functions, which represent the transverse parts of the wave functions of a free electron in a magnetic field and are the same for the solutions of the Schrödinger and Dirac equations. Therefore, this technique can be used for the ordinary ( $\hbar\omega_{ce} < m_e c^2$ ) as well as superstrong fields ( $\hbar\omega_{ce} > m_e c^2$ ), provided the atomic binding energy  $\ll m_e c^2$ , which is always the case at  $B \lesssim 10^{15}$  G.

An atom moving across the strong magnetic field acquires a constant dipole moment perpendicular to  $\mathbf{B}$  and  $\mathbf{K}$ . Those radiative transitions, which were dipole-forbidden for an atom at rest because of conservation of the  $z$ -projection of the angular momentum, become allowed and should be taken into account in the atmosphere models. The binding energies decrease with increasing  $K_{\perp}$ . Asymptotically, at large  $K_{\perp}$ , the binding energies tend to  $e^3 B / (cK_{\perp})$ .

The equation of state for partially ionized hydrogen in strong magnetic fields was constructed and discussed by Potekhin et al. (1999). The treatment is based on the free energy minimization. The free energy model is in essence a generalization of the nonmagnetic model of Saumon & Chabrier (1991, 1992) to the case of a strong magnetic field. We consider a plasma composed of  $N_p$  protons,  $N_e$  electrons,  $N_H$  hydrogen atoms, and  $N_{\text{mol}}$  molecules in a volume  $V$ , the number densities being  $n_j \equiv N_j/V$ . The Helmholtz free energy is written as the sum

$$F = F_{\text{id}}^e + F_{\text{id}}^p + F_{\text{id}}^{\text{neu}} + F_{\text{ex}}^C + F_{\text{ex}}^{\text{neu}}, \quad (1)$$

where  $F_{\text{id}}^e$ ,  $F_{\text{id}}^p$ , and  $F_{\text{id}}^{\text{neu}}$  are the free energies of ideal gases of the electrons, protons, and neutral species, respectively,  $F_{\text{ex}}^C$  takes into account the Coulomb plasma nonideality, and  $F_{\text{ex}}^{\text{neu}}$  is the nonideal contribution that arises from interactions of bound species with each other and with the electrons and protons. Ionization equilibrium is given by minimization of  $F$  with respect to particle numbers under the stoichiometric constraints, keeping  $V$  and the total number  $N_0$  of protons (free and bound) constant. The latter number is determined by the total mass density  $\rho$ :  $n_0 \equiv N_0/V \approx \rho/m_H$ , where  $m_H = m_e + m_p$ . The formulae for each term in equation (1) are given in Potekhin et al. (1999) and in Paper I. The employed minimization technique is similar to the technique presented by Potekhin (1996) for the nonmagnetic case.

Once the free energy is obtained, its derivatives over  $\rho$  and  $T$  and their combinations provide the other thermodynamic functions.

The atomic number fraction  $x_H = n_H/n_0$  evaluated in the course of the free energy minimization can be used in calculations of atmospheric opacities. One should take into

account that the strong magnetic field affects the polarization properties of radiation (e.g., Ginzburg 1970). At photon energies  $\hbar\omega$  much higher than  $(4\pi\hbar^2 e^2 n_e / m_e)^{1/2} \approx 28.7\rho_0^{1/2}$  eV, where  $\rho_0 \equiv \rho/(1 \text{ g cm}^{-3})$ , radiation propagates in the form of two so-called normal modes. These modes have different polarization vectors  $\mathbf{e}_j$  and different absorption and scattering coefficients, which depend on the angle  $\theta_B$  between the propagation direction and  $\mathbf{B}$  (e.g., Kaminker, Pavlov, & Shibanov 1982). The two modes interact with each other via scattering. Gnedin & Pavlov (1973) formulated the radiative transfer problem in terms of these modes.

Let the magnetic field be directed along the  $z$ -axis. At a fixed photon frequency  $\omega$ , the absorption opacity  $\kappa_j^a(\theta_B)$  in each mode  $j$  and scattering opacities  $\kappa_{jj'}^s(\theta_B)$  from mode  $j$  into mode  $j'$  can be presented as (e.g., Kaminker et al. 1982)

$$\kappa_j^a(\theta_B) = m_H^{-1} \sum_{\alpha=-1}^1 |e_{j,\alpha}(\theta_B)|^2 \sigma_{\alpha}^a, \quad (2)$$

$$\kappa_{jj'}^s(\theta_B) = \frac{3}{4} \sum_{\alpha=-1}^1 |e_{j,\alpha}(\theta_B)|^2 \frac{\sigma_{\alpha}^s}{m_H} \int_0^{\pi} |e_{j',\alpha}(\theta'_B)|^2 \sin \theta'_B d\theta'_B, \quad (3)$$

where  $\alpha = 0, \pm 1$ ,  $e_{j,0} = e_{j,z}$  is the  $z$ -component of  $\mathbf{e}_j$ , and  $e_{j,\pm 1} = (e_{j,x} \pm i e_{j,y})/\sqrt{2}$  are the circular components. The cross sections  $\sigma_{\alpha}$  depend on  $\omega$ , but not on  $j$  or  $\theta_B$ .

The total scattering opacity from mode  $j$  is  $\kappa_j^s = \kappa_{j1}^s + \kappa_{j2}^s$ , and the total extinction opacity is  $\kappa_j = \kappa_j^a + \kappa_j^s$ . According to equations (2) and (3), we can write

$$\kappa_j(\theta_B) = \sum_{\alpha=-1}^1 |e_{j,\alpha}(\theta_B)|^2 \hat{\kappa}_{\alpha}, \quad (4)$$

where  $\hat{\kappa}_{\alpha}$  ( $\alpha = -1, 0, 1$ ) do not depend on  $\theta_B$ . To within a good accuracy,  $\hat{\kappa}_{\alpha} \approx (\sigma_{\alpha}^a + \sigma_{\alpha}^s)/m_H$ .

In a partially ionized atmosphere, the opacity is contributed by electrons, ions, and bound species. The scattering cross section includes contributions from the electrons and protons:  $\sigma_{\alpha}^s = \sigma_{\alpha}^{s,e} + \sigma_{\alpha}^{s,p}$ . With a good accuracy,  $\sigma_{\alpha}^{s,e}$  and  $\sigma_{\alpha}^{s,p}$  are described by simple analytical formulae (e.g., Pavlov et al. 1995). The absorption cross section  $\sigma_{\alpha}^a$  includes contributions from absorption by plasma electrons and protons (mainly by free-free transitions due to the electron-proton collisions,  $\sigma_{\alpha}^{\text{ff}}$ ), transitions between discrete states of an atom (bound-bound absorption,  $\sigma_{\alpha}^{\text{bb}}$ ) and photoionization (bound-free,  $\sigma_{\alpha}^{\text{bf}}$ ). Thus, for the hydrogen atmosphere, we can write

$$\sigma_{\alpha}^a \approx x_H(\sigma_{\alpha}^{\text{bb}} + \sigma_{\alpha}^{\text{bf}}) + (1 - x_H)\sigma_{\alpha}^{\text{ff}}. \quad (5)$$

For the hydrogen atoms, electrons, and protons moving in a strong magnetic field, the cross sections  $\sigma_{\alpha}^{\text{bb}}$  were studied by Pavlov & Potekhin (1995),  $\sigma_{\alpha}^{\text{bf}}$  by Potekhin & Pavlov (1997), and  $\sigma_{\alpha}^{\text{ff}}$  in Paper I.

Ho & Lai (2003) presented convenient formulae for  $|e_{j,\alpha}(\theta_B)|^2$  for a fully ionized, strongly magnetized electron-ion plasma (taking into account vacuum polarization). However, the bound species affect the dielectric tensor of the medium and hence the polarization properties of the normal modes. For a completely neutral hydrogen gas in a strong magnetic field, polarization modes were studied by Bulik & Pavlov (1996), but

for a partially ionized gas, the problem is not yet solved. For the time being, we use the formulae of Ho & Lai (2003). Since the neutral fraction is typically small, we expect that the resulting error should not be large for the effective Rosseland mean opacities presented in the tables.

### 3. RESULTS

#### 3.1. Calculation of Tables

Since our model of the ionization equilibrium and equation of state is computationally expensive, it is not possible to use our computer code on-line in any practical application. The alternative is to tabulate thermodynamic quantities covering the density, temperature, and magnetic field domain of interest and to rely on an interpolation of the tabular values. In Paper I, we presented tables that cover a range of  $\rho$ ,  $T$ , and  $B$  appropriate for most typical neutron stars, such as isolated radio pulsars. We used the fitting formulae for the binding energies, quantum mechanical sizes, oscillator strengths, and electron collision widths derived by Potekhin (1998). Calculations at  $B \gtrsim 10^{13.5}$  G were hampered by the absence of the relevant fits.

In order to overcome this difficulty, in the present work we have calculated the tables of the required atomic quantities as functions of the transverse pseudomomentum  $K_{\perp}$  using the computer code described by Potekhin (1994). A representative grid of  $\approx 50$  equally spaced values of  $\log K_{\perp}$  has been used for every relevant set of atomic quantum numbers and every considered field strength. Handling of these tables is easier with superstrong than with weaker fields, because the number of involved discrete states is smaller. For example, there remain no bound states with  $s = 2$  and  $s = 1$  at  $B > 2 \times 10^{13}$  G and  $B > 6 \times 10^{13}$  G, respectively. The latter point is illustrated by Figure 1, which shows the energies of the most important atomic transitions at  $K_{\perp} = 0$  as functions of  $B$ . With increasing  $B$ , the tightly bound levels  $s = 3, 2,$  and  $1$  consecutively merge with the continuum and cease to contribute to the bound-bound spectrum; instead, they appear as autoionization resonances. There still remain excited loosely bound states (with  $s = 0$  and any  $\nu$ ) at any  $B$ , but at the typical neutron star atmosphere densities, most of them are destroyed by interactions with surrounding particles.

We use a cubic interpolation across these precalculated tables in our computer code for obtaining the number fractions of atoms and molecules, thermodynamic functions, and cross sections  $\sigma_{\alpha}^{\text{bb}}$ . As previously, we employ the approximate expression for  $\sigma_{\alpha}^{\text{ff}}$  [Eq. (51) in Paper I] and numerical tables of  $\sigma_{\alpha}^{\text{bf}}$  as functions of  $K_{\perp}$  and  $\omega$  (§ 4.2 of Paper I).

In this way we have calculated and tabulated thermodynamic functions and opacities of the hydrogen plasma at  $13.5 \leq \log B[\text{G}] \leq 15.0$  (preliminary results for  $B = 10^{14}$  G were presented by Chabrier, Douchin, & Potekhin 2002). We have also updated the FORTRAN program for the cubic-polynomial interpolation of the tabulated data in the three-parameter space of  $B$ ,  $T$ , and  $\rho$ .<sup>3</sup>

As discussed by Potekhin et al. (1999), our model becomes less reliable at relatively low  $T$  and high  $\rho$ , particularly because the molecules and chains  $H_n$  are treated in an approximate manner. In this domain, the partial number fractions and thermodynamic quantities are strongly model-dependent. The stronger the magnetic field, the higher the

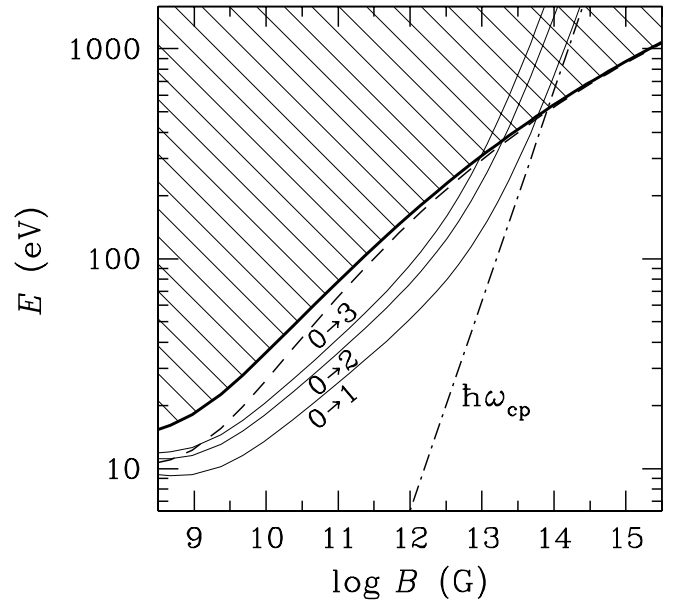


FIG. 1.—Energies of radiative transitions for the H atom with  $K_{\perp} = 0$  from the ground state to the lowest tightly bound states ( $\nu = 0, s = 1, 2, 3$ ; light solid lines) and loosely bound state ( $s = 0, \nu = 1$ ; dashed line), the photoionization threshold (heavy solid line), and the energy of the proton cyclotron resonance (dot-dashed line). The hatched region corresponds to the bound-free transitions.

temperature below which the molecules and chains dominate (Lai 2001). Trying to avoid the domain of uncertainty, we shifted the lower bound on the temperature in the tables, as compared to the case of weaker fields (Paper I), from  $2 \times 10^5$  to  $5 \times 10^5$  K. On the other hand, the temperature at which the atoms become thermally ionized increases with increasing  $B$ , therefore we have shifted the upper temperature bound in the tables from  $10^7$  to  $4 \times 10^7$  K. It would be meaningless to consider still higher  $T$ , because hydrogen undergoes efficient thermonuclear burning at such temperatures (Ergma 1986). The third input parameter in our tables, in addition to  $B$  and  $T$ , is the “astrophysical density parameter”  $R = \rho_0 / T_6^3$ , where  $T_6 = T / 10^6$  K. In order to avoid the rather uncertain region of possible phase separation (see below), we restricted the public tables by  $\log R \leq 3.4$ , although higher  $R$  values were also considered. This range of  $R$  should be sufficient for modeling the atmospheres of most neutron stars, except the unusually cold ones mentioned below.

Along with the pressure, our tables contain internal energy, entropy, specific heat, and the logarithmic derivatives of pressure with respect to  $V$  and  $T$ . Other second-order thermodynamic quantities can be calculated using the Maxwell relations (Landau & Lifshitz 1993).

The format of the tables is the same as in Paper I. In addition to the thermodynamic quantities, the tables contain the number fractions of different chemical species and also the effective Rosseland mean opacities for diffusion of radiation along and across the magnetic field.

#### 3.2. Ionization Equilibrium and Equation of State

A strong magnetic field generally increases the fraction of bound species at a given  $T$ . Figure 2 illustrates this point. In this figure, ionization equilibrium curves are plotted as functions of density for different values of  $B$  and  $T$ . At the

<sup>3</sup> The tables and the program are available at <http://www.ioffe.ru/astro/NSG/Hmagnet/>.

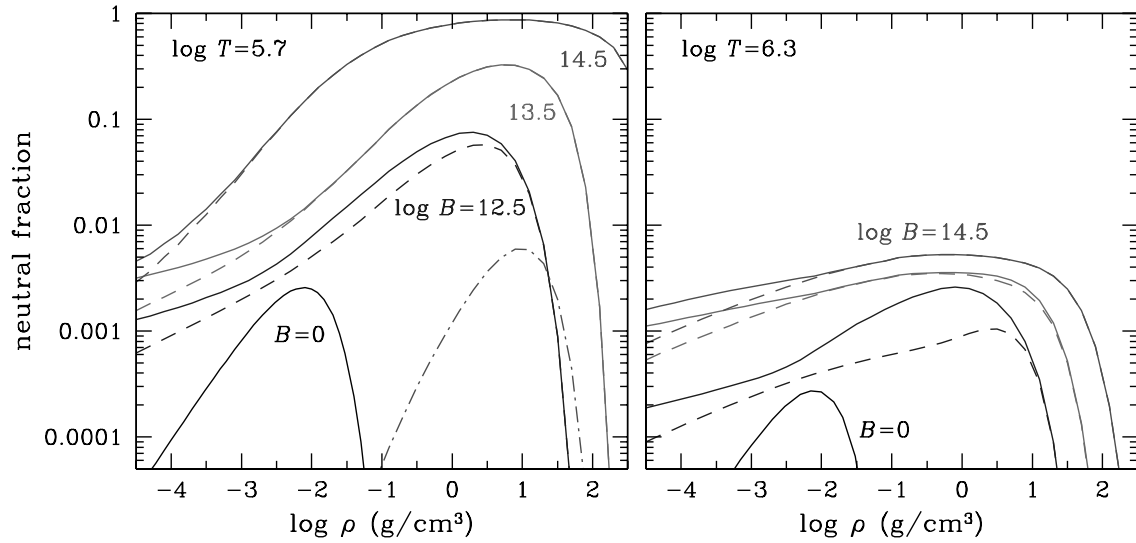


FIG. 2.—Neutral fraction of the H atoms in all quantum states (*heavy lines*) and in the ground state (*dashed lines*) as a function of density at the magnetic field strength  $B = 0, 10^{12.5} \text{ G}, 10^{13.5} \text{ G},$  and  $10^{14.5} \text{ G}$ . The dot-dashed line shows the fraction of  $\text{H}_2$  molecules at the highest  $B$ . *Left panel:*  $T = 5 \times 10^5 \text{ K}$ ; *right panel:*  $T = 2 \times 10^6 \text{ K}$ . [See the electronic edition of the *Journal* for a color version of this figure.]

lowest  $T$  and highest  $B$  shown in Figure 2, the molecular  $\text{H}_2$  fraction (dot-dashed line on the left panel) becomes significant at  $\rho \gtrsim 1 \text{ g cm}^{-3}$ . At the same  $T$  and  $B$  and higher density  $\rho \sim 100 \text{ g cm}^{-3}$ , the  $\text{H}_2$  molecules disappear, but the  $\text{H}_n$  chains and clusters (not shown in the figure) become abundant. As mentioned above, our results are not well justified under such conditions.

Figure 3 shows the domains of partial ionization in the  $T$ - $\rho$  plane at three values of  $B$ . With increasing  $B$ , the domains where the atomic fraction is above a specified level expand significantly toward higher temperatures.

Figure 4 shows pressure  $P$  as a function of  $\rho$  at  $T = 10^{6.5} \text{ K}$  and at different field strengths. At very low  $\rho$ , we have a nearly fully ionized, almost ideal nondegenerate gas of electrons and protons. The magnetic field does not affect the equation of state in this case. With increasing density, at  $10^2 \text{ g cm}^{-3} \lesssim \rho \lesssim 10^3 \text{ g cm}^{-3}$ , the electrons become degenerate at  $B = 0$ , but remain nondegenerate at  $B \gtrsim 10^{12} \text{ G}$ . This explains why the dashed line in the figure (pressure at  $B = 0$ ) is higher than the other lines in this regime. Meanwhile, because of the partial recombination of atoms, the solid curves ( $P$  of the nonideal

magnetized plasma) are slightly lower than the dotted ones ( $P$  of the ideal fully ionized plasma). At still higher density, however, the atoms become pressure ionized; in this region, the increase of  $P$  due to the increased number of free electrons and protons competes with a negative nonideal contribution, which is mainly due to the Coulomb term  $F_{\text{ex}}^{\text{C}}$  in the free energy.

At sufficiently high  $B$  or low  $T$ , the Coulomb interaction leads to a discontinuity, exemplified in Figure 4 by the line  $B = 10^{15} \text{ G}$ . It occurs at  $T$  below the critical temperature  $T_c$  and at  $\rho$  around the critical density  $\rho_c \approx 143B_{12}^{1.18} \text{ g cm}^{-3}$  (Potekhin et al. 1999), where  $B_{12} = B/10^{12} \text{ G}$ . This phase transition is directly related to the magnetic field assisted separation between the condensed hydrogen and vapor discussed by Lai & Salpeter (1997). Note that the density of the condensed phase at zero pressure and zero temperature, estimated by Lai & Salpeter (1997) as  $\rho_s \approx 560B_{12}^{6/5} \text{ g cm}^{-3}$ , scales with  $B$  similarly to  $\rho_c$ . At  $B = 10^{15} \text{ G}$ , this estimate gives  $\rho_s \approx 2.2 \times 10^6 \text{ g cm}^{-3}$ , whereas we have numerically  $\rho_s \approx 1.7 \times 10^6 \text{ g cm}^{-3}$  in Figure 4. However, in general, the validity of the free-energy models in the framework of the chemical picture of plasmas is questionable near the plasma phase transition. In

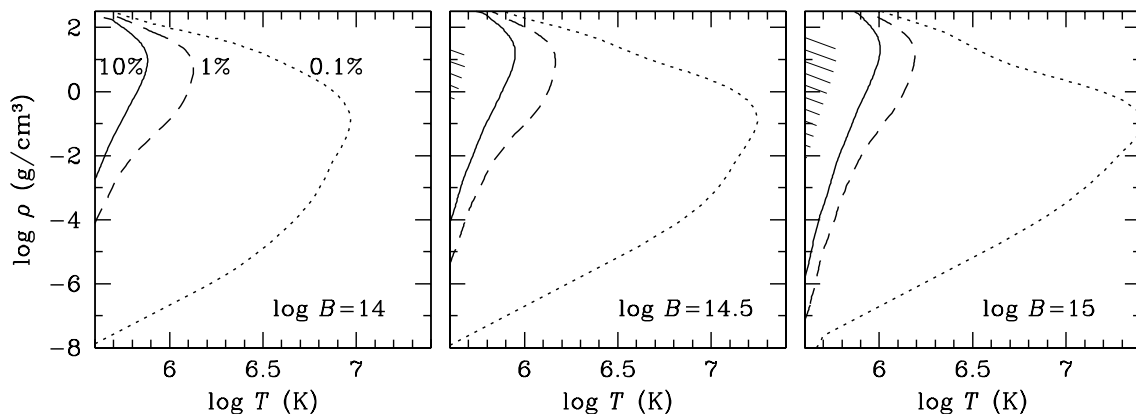


FIG. 3.—Domains of partial ionization at  $\log B[\text{G}] = 14.0, 14.5,$  and  $15.0$ . The contours delimit the domains where the atomic fraction exceeds 0.1% (*dotted lines*), 1% (*dashed lines*), or 10% (*solid lines*). The hatched domain is where the  $\text{H}_2$  fraction exceeds 1%.

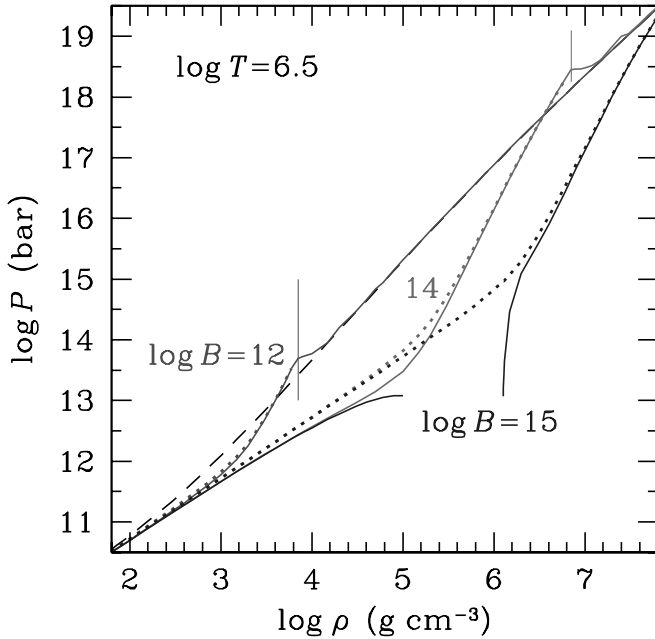


FIG. 4.—Pressure isotherms ( $T = 10^{6.5}$  K) of partially ionized hydrogen in the strong magnetic field ( $B = 10^{12}$ ,  $10^{14}$ , and  $10^{15}$  G; *solid lines*) compared with the model of a fully ionized ideal electron-proton plasma (*dotted lines*) and with the case of a hydrogen plasma at  $B = 0$  (*dashed line*). The vertical lines correspond to the density above which excited Landau levels become populated. The instability region at  $B = 10^{15}$  G (*discontinuity of the lower solid curve*) corresponds to a hypothetical plasma phase transition (see text). [See the electronic edition of the Journal for a color version of this figure.]

order to study the matter properties near the phase transition, one needs to consider accurately the interaction of  $H_n$  molecules in the gas phase and their interaction with the surface of the condensed phase. This problem goes beyond the scope of the present paper, although it certainly deserves a future study. If this phase separation is real, it can be important for

interpretation of the emission of neutron stars with unusually low  $T$  and/or high  $B$ , which in this case do not possess an optically thick atmosphere above the condensed surface. This hypothesis was suggested by Lai & Salpeter (1997); a possible example of such a “naked neutron star” has been recently considered by Turolla et al. (2003).

### 3.3. Opacities

Figure 5 shows the monochromatic extinction coefficients  $k_\alpha = \rho \hat{\kappa}_\alpha$  for the three basic polarizations  $\alpha = 0, \pm 1$  at  $B = 10^{13.5}$  G,  $T_6 = 1$  or 4, and  $\rho = 0.1$  g cm $^{-3}$  or 50 g cm $^{-3}$ . Figure 6 demonstrates the same functions for 10 times higher magnetic field and densities. These densities correspond to the outer and inner layers of the atmosphere, where the optical depth is of the order of 1 for ordinary (high-opacity) and extraordinary (low-opacity) modes of radiation, respectively (see, e.g., Ho & Lai 2003). At the higher densities, the opacities are featureless, except the proton cyclotron resonance at  $\hbar\omega_{cp} = \hbar\omega_{ce}m_e/m_p = 6.305B_{12}$  eV, because the plasma at such density is pressure ionized. On the contrary, absorption features are clearly visible at the lower density.

At the lower field strength (Fig. 5), one sees the broad absorption feature for  $\alpha = \pm 1$  (*left and central panels*) due to the  $s = 0 \rightarrow 1$  bound-bound transition at  $\hbar\omega \lesssim 0.3$  keV. For  $\alpha = +1$  (Fig. 5, *left panel*), this absorption merges with the strong proton cyclotron free-free resonance at lower energies and with the photoionization continuum at higher energies. This situation is rather special, because at this field strength  $\hbar\omega_{cp}$  is rather close to the photoionization threshold, whereas the limiting energy for the bound-bound transition falls in between (see Fig. 1). Both the photoionization edge and the absorption line are considerably broadened because of the energy shifts due to the atomic motion (the magnetic broadening; see Pavlov & Potekhin 1995; Potekhin & Pavlov 1997), therefore they effectively merge together. On the other hand, the free-free absorption coefficient at the lower  $T$  (Fig. 5, *solid curve*) reveals the bumps at  $\hbar\omega \lesssim 1$  keV, which arise from the

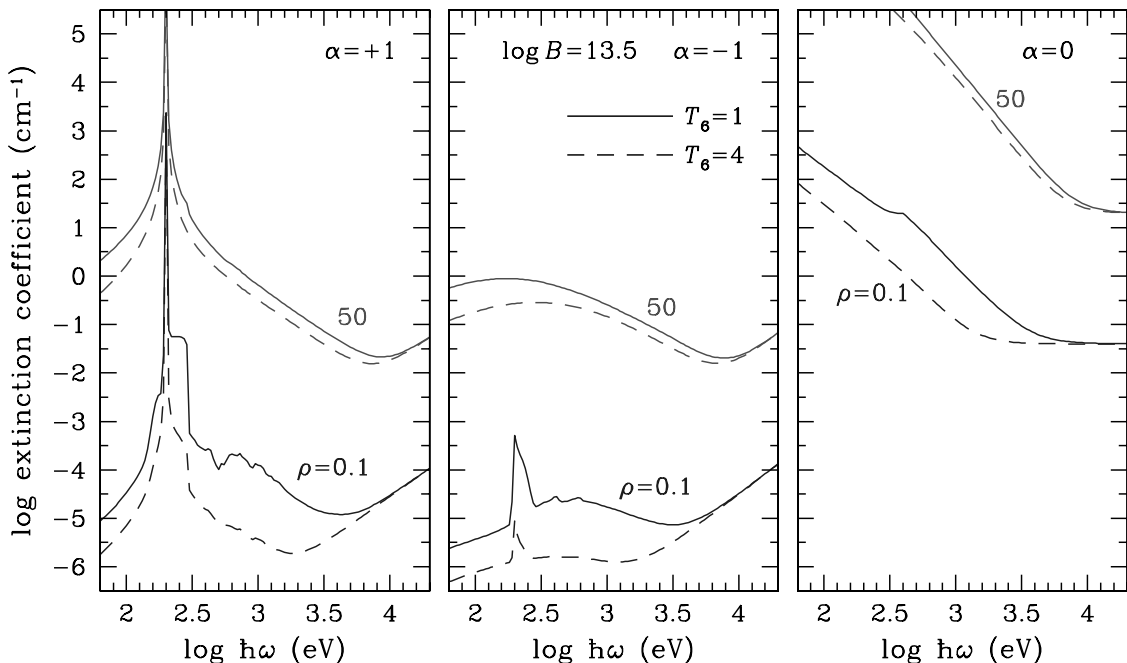


FIG. 5.—Monochromatic extinction coefficients for the three basic polarizations,  $k_\alpha = \rho \hat{\kappa}_\alpha$ ,  $\alpha = 0, \pm 1$ , at  $\rho = 0.1$  and 50 g cm $^{-3}$ ,  $T = 10^6$  (*solid lines*) and  $4 \times 10^6$  K (*dashed lines*),  $B = 10^{13.5}$  G. [See the electronic edition of the Journal for a color version of this figure.]

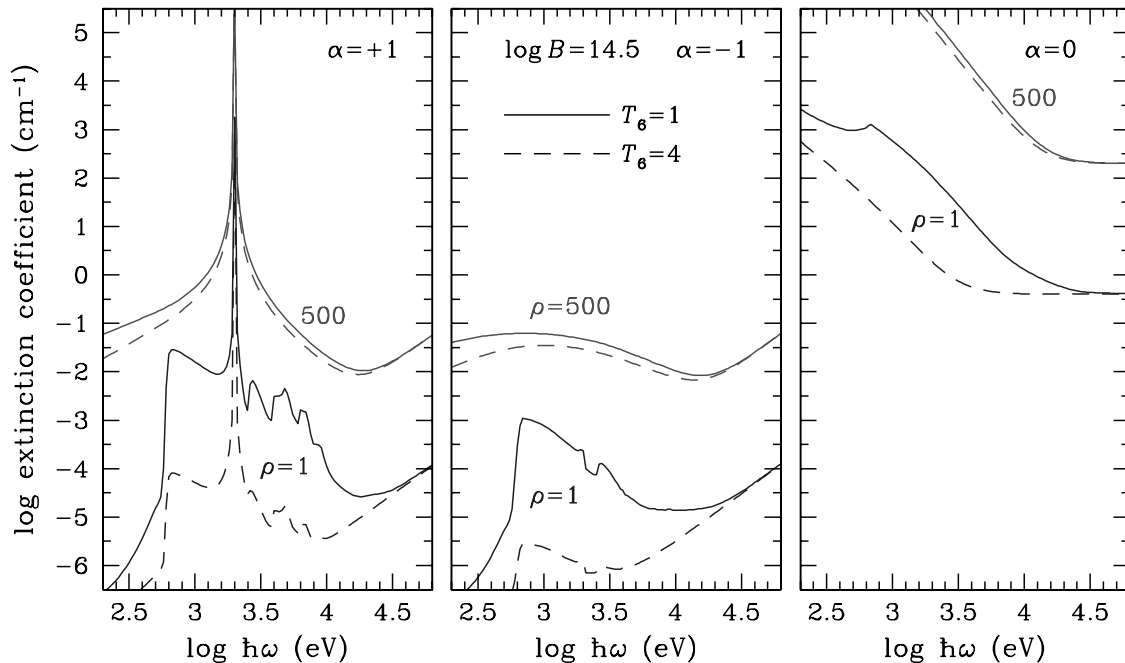


Fig. 6.—The same as in Fig. 5, but for  $\rho = 1 \text{ g cm}^{-3}$  and  $500 \text{ g cm}^{-3}$ ,  $B = 10^{14.5} \text{ G}$ . [See the electronic edition of the Journal for a color version of this figure.]

opening of ionization channels with higher  $s$  values at higher energies and from autoionization resonances just below these partial ionization thresholds (Potekhin & Pavlov 1997). On the right panel of Figure 5 ( $\alpha = 0$ , the polarization vector along  $\mathbf{B}$ ), one notices only the photoionization edge at relatively small  $\rho$  and  $T$  (lower solid line).

At the higher field strength (Fig. 6), all transitions changing  $s$  belong to the continuum (see Fig. 1) and form a series of resonances on the photoionization profile at the energies above  $\hbar\omega_{\text{cp}}$ , which are particularly visible for  $\alpha = +1$  at low  $\rho$  and  $T$  (left panel, lower solid line). Near the bottom of the photosphere ( $\rho = 500 \text{ g cm}^{-3}$ ), the bound states are destroyed and do not contribute to the spectrum.

#### 4. CONCLUSIONS AND OUTLOOK

We have calculated the equation of state of fully and partially ionized hydrogen plasmas in a wide range of densities, temperatures, and magnetic fields expected for photospheres of the magnetars. We have also calculated monochromatic radiative opacities for three basic polarizations. The first- and second-order thermodynamic functions, non-ionized fractions, and effective Rosseland mean opacities are published in electronic form at the Ioffe Physico-Technical Institute Neutron Star Group EOS and opacities Web page.<sup>4</sup>

These results can be useful for construction of atmosphere models and calculation of spectra of outgoing radiation from warm neutron stars with superstrong magnetic fields. This work is underway; some results have been published by Ho et al.

<sup>4</sup> See <http://www.ioffe.ru/astro/NSG/Hmagnet/>.

(2003a, 2003b). However, there remain unsolved problems that hamper an immediate application of our present results to modeling accurate and reliable emission spectra of magnetars with hydrogen atmospheres. First, vacuum polarization alters the dielectric tensor of the medium and polarization of photon modes (see Pavlov & Gnedin 1984). This effect is important for magnetar atmospheres. In particular, the “vacuum resonance” phenomenon may lead, under certain conditions, to an adiabatic mode conversion and “mode collapse” (Ho & Lai 2003 and references therein). In the latter case, the description in terms of the two modes fails, and one has to solve more general equations for the evolution of electromagnetic waves (Lai & Ho 2003). Second, as noted in § 2, the presence of the bound species also changes the dielectric properties of the medium and the normal mode polarization, which necessitates derivation of a polarization tensor for partially ionized, strongly magnetized plasmas. Third, for relatively cold neutron stars with strong magnetic fields, the phase separation mentioned in § 3.2 should be studied in a thermodynamically consistent way. We are planning to study these problems in the near future.

We thank Dong Lai for useful discussions and Yura Shibano and Wynn Ho for valuable remarks. A. P. gratefully acknowledges the hospitality of the theoretical astrophysics group at the Ecole Normale Supérieure de Lyon and the Astronomy Department of Cornell University. The work of A. P. is supported in part by RFBR grants 02-02-17668 and 03-07-90200.

#### REFERENCES

- Bulik, T., & Pavlov, G. G. 1996, *ApJ*, 469, 373  
 Canuto, V., & Ventura, J. 1977, *Fundam. Cosmic Phys.*, 2, 203  
 Chabrier, G., Douchin, F., & Potekhin, A. Y. 2002, *J. Phys. Condensed Matter*, 14, 9133  
 Ergma, E. 1986, *Astrophys. Space Phys. Rev.*, 5, 181  
 Ginzburg, V. L. 1970, *The Propagation of Electromagnetic Waves in Plasmas* (2d ed.; Oxford: Pergamon)  
 Gnedin, Yu. N., & Pavlov, G. G. 1973, *Zh. Eksper. Teor. Fiz.*, 65, 1806 (English transl. in *Sov. Phys.-JETP*, 38, 903 [1974])  
 Gor'kov, L. P., & Dzyaloshinskii, I. E., 1967, *Zh. Eksper. Teor. Fiz.*, 53, 717 (English transl. in *Sov. Phys.-JETP*, 26, 449 [1968])  
 Ho, W. C. G., & Lai, D., 2003, *MNRAS*, 338, 233  
 Ho, W. C. G., Lai, D., Potekhin, A. Y., & Chabrier, G. 2003a, *Adv. Space Res.*, in press (astro-ph/0212077)

- Ho, W. C. G., Lai, D., Potekhin, A. Y., & Chabrier, G. 2003b, *ApJ*, 599, 1293
- Ipatova, I. P., Maslov, A. Y., & Subashiev, A. V. 1984, *Zh. Eksper. Teor. Fiz.*, 87, 1804 [English transl. in *Sov. Phys.-JETP*, 60, 1037]
- Kaminker, A. D., Pavlov, G. G., & Shibano, Yu. A. 1982, *Ap&SS*, 86, 249
- Lai, D. 2001, *Rev. Mod. Phys.*, 73, 629
- Lai, D., & Ho, W. C. G. 2003, *ApJ*, 588, 962
- Lai, D., & Salpeter, E. E. 1997, *ApJ*, 491, 270
- Landau, L. D., & Lifshitz, E. M. 1993, *Statistical Physics, Part 1* (Oxford: Pergamon)
- Özel, F. 2003, *ApJ*, 583, 402
- Page, D., Shibano, Yu. A., & Zavlin, V. E. 1996, in *Röntgenstrahlung from the Universe*, ed. H. U. Zimmermann, J. E. Trümper, & H. Yorke (MPE Rep. 263; Garching: MPE), 173
- Pavlov, G. G., & Gnedin, Yu. N. 1984, *Astrophys. Space Phys. Rev.*, 3, 197
- Pavlov, G. G., & Potekhin, A. Y. 1995, *ApJ*, 450, 883
- Pavlov, G. G., Shibano, Yu. A., Zavlin, V. E., & Meyer, R. D. 1995, in *NATO ASI Ser. C 450, The Lives of the Neutron Stars*, ed. M. A. Alpar, Ü. Kiziloğlu, & J. van Paradijs (Dordrecht: Kluwer), 71
- Potekhin, A. Y. 1994, *J. Phys. B*, 27, 1073
- . 1996, *Phys. Plasmas*, 3, 4156
- . 1998, *J. Phys. B*, 31, 49
- Potekhin, A. Y., & Chabrier, G. 2003, *ApJ*, 585, 955 (Paper I)
- Potekhin, A. Y., Chabrier G., & Shibano, Yu. A. 1999, *Phys. Rev. E*, 60, 2193
- Potekhin, A. Y., & Pavlov, G. G. 1997, *ApJ*, 483, 414
- Saumon, D., & Chabrier, G. 1991, *Phys. Rev. A*, 44, 5122
- . 1992, *Phys. Rev. A*, 46, 2084
- Shibano, Yu. A., Pavlov, G. G., Zavlin, V. E., & Ventura, J. 1992, *A&A*, 266, 313
- Thompson, C. 2003, *Mem. Soc. Astron. Italiana*, 73, 477
- Turolla, R., Zane, S., & Drake, J. 2003, *ApJ*, in press (astro-ph/0308326)
- Vincke, M., Le Dourneuf, M., & Baye, D. 1992, *J. Phys. B*, 25, 2787
- Zane, S., Turolla, R., Stella, L., & Trevis, A., 2001, *ApJ*, 560, 384
- Zavlin, V. E., Pavlov, G. G., Shibano, Yu. A., & Ventura, J. 1995, *A&A*, 297, 441